Malaysian Journal of Chemistry, 2026, Vol. 28(2), 377-390
(Special Issue: *1st International Conference on Chemical and Energy Engineering 2025, ICChEE2025*)

MXene Immobilized PVDF Photocatalytic Membrane for Palm-Oil Mill Effluent Treatment

Tharmahavel K. Ravichandaran, Nur Husnina Arsad and Juhana Jaafar*
Advanced Membrane Technology Research Centre (AMTEC), Faculty of Chemical and Energy Engineering, Universiti Teknologi Malaysia, 81310 Skudai, Johor, Malaysia
*Corresponding author (e-mail: juhana@petroleum.utm.my)

Palm oil mill effluent (POME) is a highly polluted industrial wastewater containing elevated chemical oxygen demand (COD) and suspended solids, requiring advanced and sustainable treatment technologies beyond conventional methods. In this study, polyvinylidene fluoride (PVDF) membranes immobilized with varying loadings of MXene (Ti_2C) photocatalytic nanofibers were fabricated and evaluated for palm oil mill effluent (POME) treatment. The results demonstrated that increasing MXene loading improved nanofiber diameter, surface hydrophilicity, and both water and POME flux; however, excessive loading (5 wt%) induced MXene agglomeration and excessive pore enlargement, which diminished COD rejection. In contrast, the membrane containing 3 wt% MXene provided an optimal balance between porosity and pore size, resulting in high COD and total suspended solids (TSS) removal together with good permeability and structural stability. Overall, the PVDF–MXene membrane containing 3 wt% MXene exhibited the most balanced performance by achieving high COD and total suspended solids (TSS) removal while maintaining good permeation flux and structural integrity, highlighting its strong potential as an efficient and sustainable membrane material for POME treatment.

Keywords: Palm-oil Mill Effluent (POME), polyvinylidene fluoride (PVDF), photocatalytic membrane, MXene

Received: July 2025; Accepted: January 2026

Palm oil mill effluent (POME) is a highly polluted industrial wastewater generated during palm oil processing and is characterized by extremely high chemical oxygen demand (COD), biochemical oxygen demand (BOD), and suspended solids. Malaysia, as the second largest producer of palm oil in the world produced 15.82 million tons of crude palm oil (CPO) in 2008 and 19.92 million tons in 2017 [1]. Although conventional treatment methods such as anaerobic ponding, integrated anaerobic–aerobic bioreactors, and zero liquid discharge systems are effective for bulk organic removal, they are often limited by long hydraulic retention times, large land requirements, and insufficient degradation of recalcitrant organic compounds [2].

In recent years, membrane technology has emerged as a promising alternative for POME treatment due to its high efficiency, compact design, and ability to handle a wide range of pollutants. Studies have shown that both ceramic and polymer membranes effectively remove suspended solids from POME, with the latter showing improved performance at higher transmembrane pressure and crossflow velocity [3]. Moreover, polyvinylidene fluoride (PVDF) is favoured for its excellent chemical resistance, thermal stability, and mechanical strength. However, PVDF membranes can suffer from fouling, which reduces their efficiency and operational lifespan. To enhance the performance of PVDF membranes, researchers have investigated the incorporation of photocatalysts, which can degrade organic pollutants under light irradiation. Photocatalytic membranes combine the separation capability of conventional membranes with the degradation functionality of photocatalysts. Of many materials that have been studied for photocatalysis, titanium dioxide (TiO_2) has been widely studied for organic pollutant degradation purpose due to its strong oxidative properties, chemical stability, non-corrosive, non-toxicity, high availability, and low cost [4]. However, TiO_2 encounter limitations in photocatalytic efficiency due to their wide band gap (3.2 eV for anatase TiO_2) and rapid recombination of photoinduced charge carriers which confines their activity to UV light [5, 6]. Hence, this challenge has prompted the investigation of alternative materials such as MXenes.

MXenes, a class of two-dimensional transition metal carbides, have recently attracted significant attention due to their high electrical conductivity, hydrophilicity, and surface-rich functional groups [7].

†Paper presented at the 1st International Conference on Chemical and Energy Engineering 2025 (ICChEE2025)

Unlike conventional photocatalysts such as TiO_2, which are primarily activated under ultraviolet irradiation, MXenes exhibit strong visible-light absorption and improved charge carrier separation, enabling more efficient photocatalytic activity under broader light conditions. These advantages allow MXenes to promote the generation and transport of reactive species for the degradation of recalcitrant organic pollutants in wastewaters such as POME [8]. Furthermore, the immobilization of MXene nanofibers onto PVDF membranes can reduce fouling propensity, and improve structural durability, thereby extending operational lifespan and making MXene-based photocatalytic membranes a promising platform for advanced POME treatment [9].

Despite the growing interest in MXene-based materials for water treatment, studies focusing on the immobilization of MXene in nanofiber form onto polymeric membranes for the simultaneous integration of filtration and photocatalytic functions in POME treatment remain limited. In particular, the effect of MXene loading on membrane morphology, pore structure, surface hydrophilicity, and overall treatment performance has not yet been systematically investigated. This gap highlights the need for a comprehensive study to establish structure–property–performance relationships for MXene-embedded nanofiber membranes in treating high-strength industrial wastewater such as POME.

This study aims to develop MXene-immobilized PVDF nanofiber membranes with varying MXene loadings and to evaluate their structural, surface, and photocatalytic-assisted filtration performance for palm oil mill effluent (POME) treatment. The influence of MXene loading on membrane morphology, hydrophilicity, pore structure, permeation flux, and contaminant removal efficiency was systematically investigated to correlate the structure, properties, and performance.

EXPERIMENTAL

Chemicals and Materials

The commercial PVDF pellets (Solef 6000 Series) was obtained from Solvay Specialty Polymers, France, to be used as the primary component in membrane formation. The selection was based on PVDF's excellent resistance to thermal and chemical degradation. Hydrofluoric acid (49 wt%), and dimethylformamide (DMF, 99%), obtained from Sigma Aldrich, used as the polymer solvent. DMF is an exceptional solvent for high molecular weight polymers [10]. Titanium Aluminium Carbide ($Ti_2AlC \geq 99$ %Ti), MAX phase powder was obtained from Luoyang Tongrun Info Technology Co., Ltd., China.

Sample Preparation Methods

Preparation of PVDF Membrane

The PVDF dope solution (18 wt%) was prepared by dissolving oven-dried PVDF powder in DMF under continuous mechanical stirring at 60 °C for 24 h until a homogeneous solution was obtained, followed by degassing to remove entrapped air bubbles prior to membrane casting. [11].

PVDF flat-sheet membranes were fabricated via non-solvent induced phase separation (NIPS) by casting the degassed dope solution onto a glass plate with a thickness of 30–40 μm, followed by immersion in a deionized water coagulation bath and subsequent soaking in water overnight prior to drying at room temperature [12].

Preparation of MXene Powder

10 g of titanium aluminium carbide ($Ti_2AlC \geq 99$ %Ti), MAX phase powder was added gradually to a 300 mL of 49 wt% HF aqueous solution in a 2500 mL schott bottle inside a fume hood. The mixture was magnetically stirred for 24 hours at room temperature with the bottle cap closed. Then, the mixture was rinsed multiple times with deionized water to raise the pH from 2.5 to between 6 and 7. The resulting mixture was centrifuged for 2 hours at 5000 rpm to remove any unexfoliated Ti_2C. The collected wet slurry in DI water was dispensed and ultrasonicated for one to two hours. The washed powder, with a neutral pH, was dried in an oven at 60 °C for 24 hours. Finally, the obtained dried powder form of MXene (without Al) stored in a freezer before use [10].

Preparation of MXene Nanofiber Membrane

To prepare the electrospinning polymeric solution, 9 g (18 wt%) of PVDF was added to 33.57 mL of DMF, creating solution A. This mixture was magnetically stirred for 2 hours in a 45 °C water bath. Simultaneously, 0.5 g (1.0 wt%) of MXene was dissolved in 6.93 ml of DMF to create solution B. Solution B was stirred for 1 hour and then ultrasonicated for 15 minutes to evenly distribute the MXene in the DMF solvent. Solution B was then combined with solution A and stirred magnetically for another hour. This process was repeated to prepare precursor solutions for nanofiber electrospinning with 3.0 wt% and 5.0 wt% of MXene [13].

Electrospinning was carried out using a high-voltage power supply and a syringe pump equipped with a 23-gauge blunt-tip needle. The precursor solution was loaded into a 10 mL syringe, and the solution flow rate was maintained at 1.5 mL h^{-1} [10].

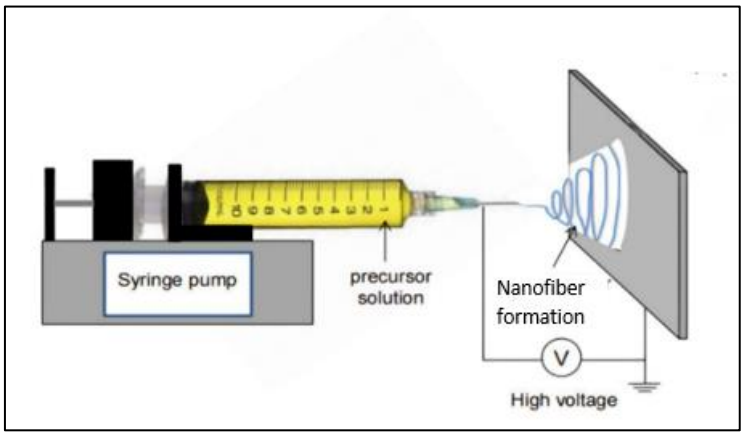

Figure 1. Electrospinning setup to produce MXene nanofiber membrane.

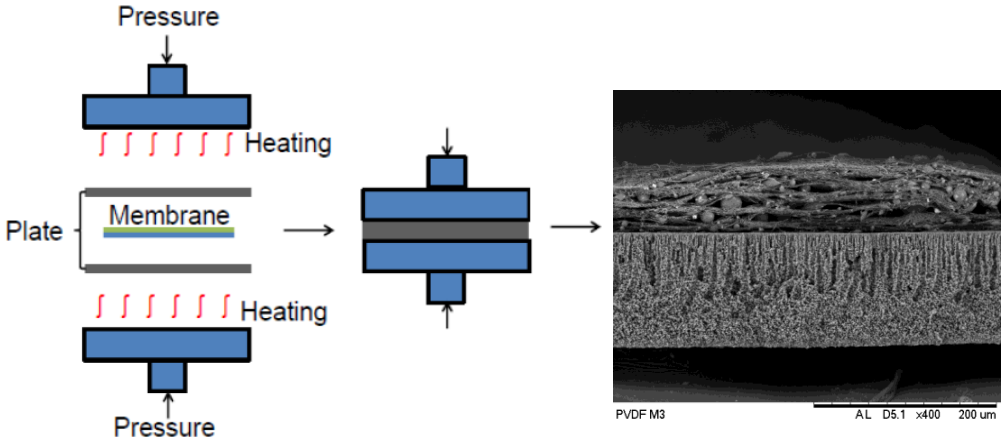

Figure 2. Hot press method.

Hot Pressing of MXene Nanofiber Membrane on PVDF Membrane

The electrospun PVDF–MXene nanofiber mat was hot-pressed onto the PVDF flat-sheet membrane using a hydraulic press. The membrane assembly was sandwiched between two clean aluminium plates to minimize contamination and ensure uniform pressure distribution. Hot pressing was conducted at 80 °C and 5 bar for 5 min, followed by cooling under compression to maintain membrane integrity (Figure 2) [10].

Characterization Methods

Scanning Electron Microscopy (SEM) and Energy-dispersive X-ray (EDX) Analysis

The morphology of the PVDF/MXene nanofiber membrane was examined using a scanning electron microscope (SEM, Hitachi TM 3000), and elemental composition was analysed via energy-dispersive X-ray spectroscopy (EDX). Membrane surfaces were mounted on stainless steel stubs with carbon tape, while cross-sectional samples were prepared by fracturing water-wetted membranes in liquid nitrogen. All samples were sputter-coated with platinum prior to imaging. SEM images were obtained at magnifications of ×500, ×1500, ×3000, and ×8000, and the average fiber diameter was measured using image analysis software.

Membrane Porosity

Membrane porosity (ε) was determined gravimetrically. Dried membranes were immersed in water at room temperature for 24 h, blotted to remove excess water, and weighed (W_w). Membranes were then dried in a vacuum oven at 70 °C for 48 h and weighed again (W_d). Porosity was calculated using equation (Eq.(1)) [14]:

$$\varepsilon\,(\%) = \frac{((Ww-Wd))/(\rho H_2O)}{\frac{(Ww-Wd)}{\rho H_2O}+\frac{Wd}{\rho PVDF}} \times 100 \quad (1)$$

where W_w is the weight of the wet membrane, W_d is the weight of the dry membrane, ρH_2O is the density of water (0.998 g/cm³), and $\rho PVDF$ is the density of PVDF (1.78 g/cm³).

Membrane Mean Pore Size

The mean pore radius (r_m) was calculated using the Guerout-Elford-Ferry equation (Eq. (2))

$$r_m\,(\%) = \sqrt{\frac{(2.9-1.7\varepsilon)x\ 8\eta lQ}{\varepsilon \times A \times \Delta P}} \times 100\% \quad (2)$$

where η is the water viscosity (8.9 x 10^{-4} Pa.s), l is the membrane thickness (m), Q is the permeate volume per time (m^3s^{-1}), A is the membrane area (m^2), and ΔP is the applied pressure (Pa).

Contact Angle Analysis

Surface hydrophilicity was evaluated by measuring the static water contact angle of a 1 µL droplet using a goniometer (OCA15Pro, Data Physics, Germany). Measurements were performed within 10 s of droplet deposition to minimize evaporation, with five replicates per sample [10].

Fourier Transform Infrared Spectroscopy (FTIR) Analysis

Membrane samples were dried in a desiccator for 24 h prior to analysis. Spectra were recorded using an FTIR instrument equipped with an attenuated total reflectance (ATR) crystal (Ge or ZnSe) at a 45° incidence angle. For each FTIR study, the spectrum was typically evaluated in the range of 760–3860 cm^{-1}.

Ultraviolet-Visible (UV-Vis) Analysis

Optical absorption of the PVDF-M nanofiber membranes was recorded using a UV–Vis–NIR spectrophotometer over a wavelength range of 380–700 nm. Samples were securely placed in the holder for scanning under ambient conditions.

Pure Water Flux

Pure water flux was measured using a dead-end filtration setup at 4 bar and 10 rpm peristaltic pump at room temperature. Membranes were pre-pressurized with deionized water for 30 min to minimize compaction. After stabilization, the lights were turned on, and the volume of permeate was recorded every 5 minutes over a one-hour period. The experimental setup is shown in Figure 3. The flux (J) was calculated using the following equation: (Eq. (3)) [14]:

$$J = \frac{V}{A \times \Delta t} \quad (3)$$

where V is the permeate volume (L), A is the effective membrane area (m^2) and Δt is the collection time (h).

Pure POME Flux

POME flux was measured under the same conditions using aerobically treated POME diluted 1:20 with deionized water. Membranes were pre-pressurized and allowed 60 min of adsorption in the dark prior to illumination. Flux was recorded every 5 min for 1 h, and calculated using the same equation as pure water flux.

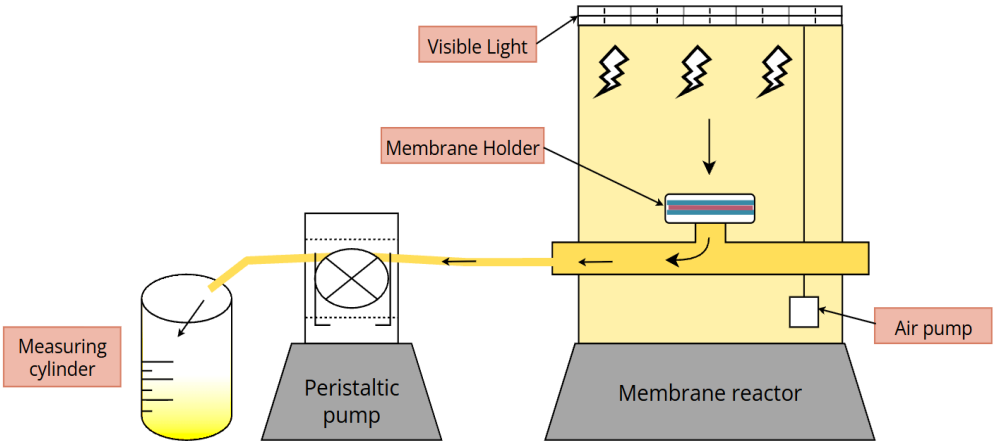

Figure 3. Experimental setup for water flux, POME flux, and COD analysis.

Chemical Oxygen Demand (COD) Analysis

COD of POME samples was determined using a COD photometer. Samples (2 mL) were pipetted into COD vials with reagent and digested at 150 °C for 2 h. COD rejection was calculated using the following equation (Eq. (4)):

$$\text{COD Rejection (\%)} = \frac{Ci - Ca}{Ci} \times 100\% \quad (4)$$

where C_i and C_a are the COD value of feed and permeate, respectively.

Total Suspended Solid (TSS) Analysis

The total suspended solid (TSS) analysis was conducted alongside the POME flux analysis, where the initial and final weights of the membranes were measured before and after the experiment. TSS was determined gravimetrically. Filters retaining solids were dried at 105 °C for 1 h, cooled for 30 min, and weighed. TSS (%) was calculated using equation (Eq. (5)):

$$\text{TSS (\%)} = \frac{(W2 - W1)}{W1} X\ 100 \quad (5)$$

where W_1 and W_2 are initial and final filter weights, respectively.

RESULTS AND DISCUSSION

Morphology and Structural Properties

SEM analysis revealed that increasing MXene loading significantly influenced the nanofiber morphology and membrane microstructure (Figure 4 and 5). The pristine PVDF nanofibers (0 wt% MXene) exhibited smooth, uniform cylindrical fibers with narrow diameter distribution, reflecting stable electrospinning. Incorporation of MXene increased fiber diameter and inter-fiber connectivity, indicating effective integration of two-dimensional MXene nanosheets within the polymer matrix. Lateral dimensions of MXene nanosheets were typically 200–600 nm, with partial agglomeration observed at higher loadings (5 wt%), forming clusters up to 900 nm.

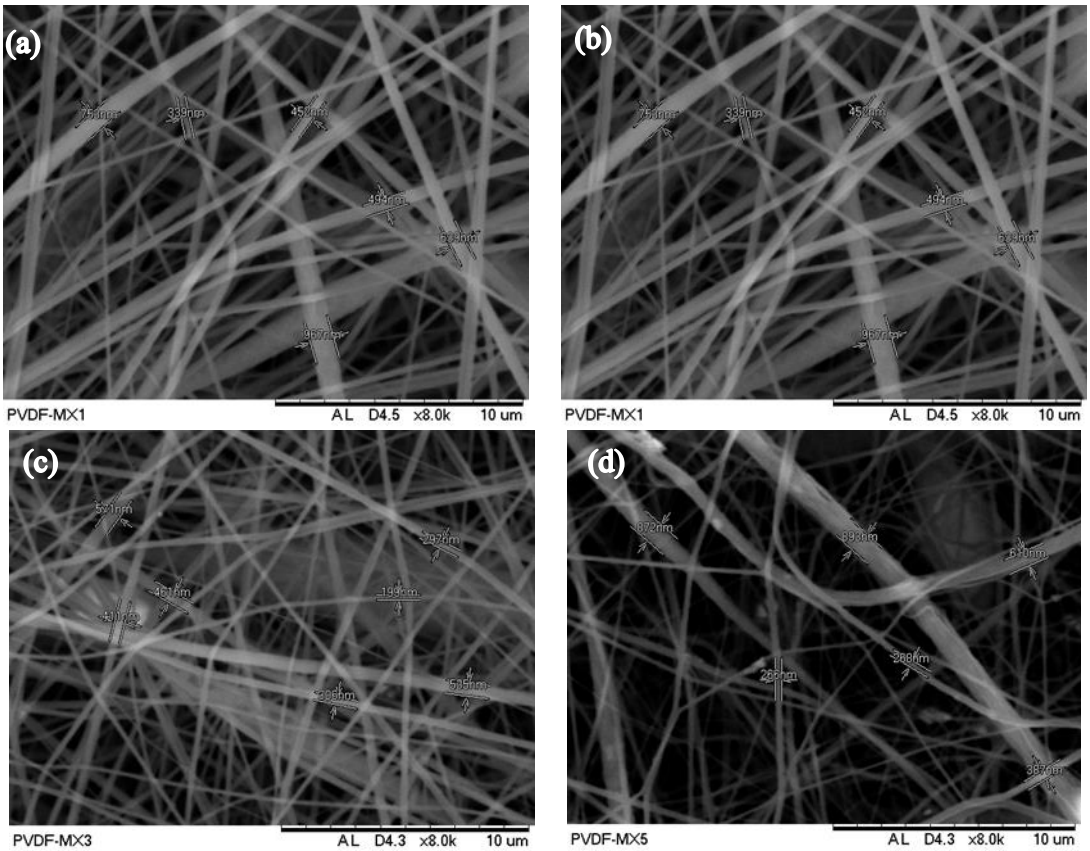

Figure 4. SEM images illustrating images and size distribution of MXene nanofibers at different loadings of MXene: a) MXene-0 wt%, b) MXene-1wt%, c) MXene-3 wt% and d) MXene-5 wt%.

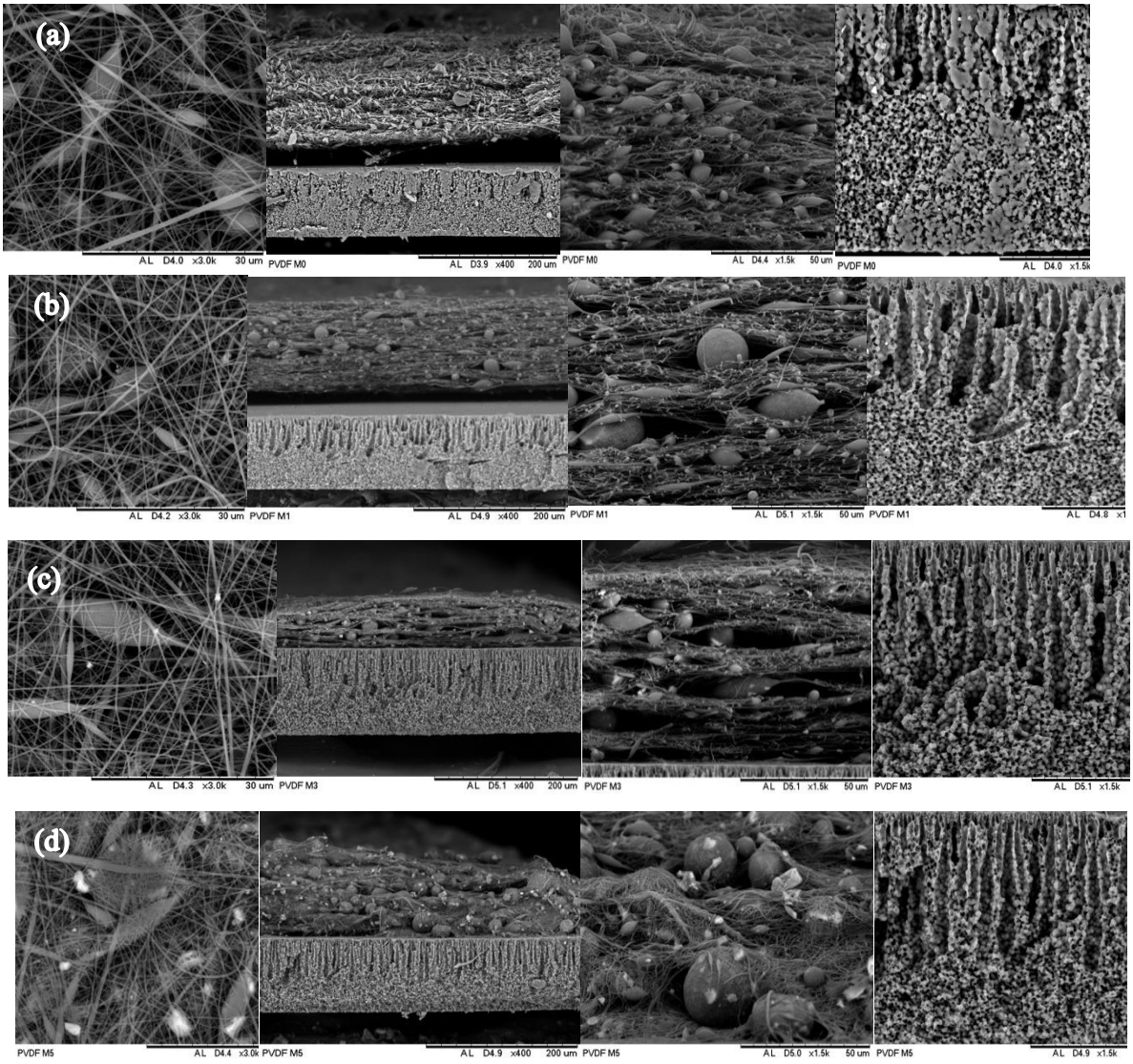

Figure 5. SEM images illustrating the surface and cross section images and size distribution of MXene nanofibers at different ratios: (a) PVDF-M 0 wt% b) PVDF-M 1 wt%, c) PVDF-M wt 3% and d) PVDF-M 5 wt%.

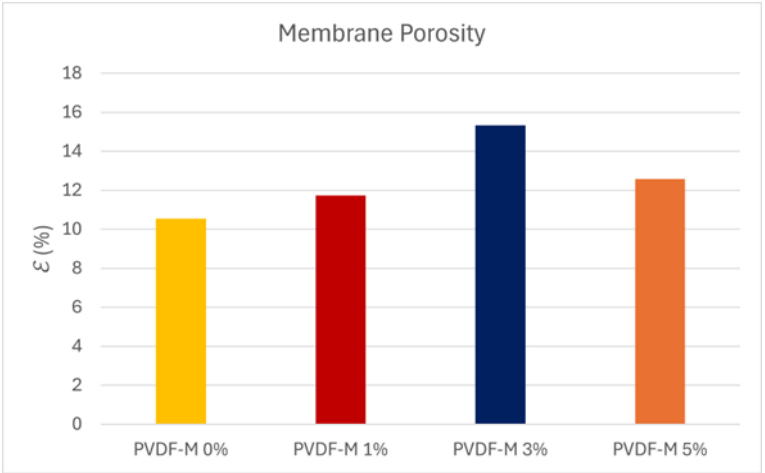

Figure 6. Data analysis for membrane porosity.

Membrane porosity and mean pore size followed trends consistent with fiber morphology (Figure 6 and 7). PVDF-M 3% exhibited a homogeneous nanofiber network with well-interconnected pores and reduced pore size, attributed to uniform MXene dispersion within the matrix [15]. In contrast, PVDF-M 5% showed pore irregularity and partial enlargement due to nanosheet agglomeration, while PVDF-M 1% displayed localized pore blockage. This combination of SEM, porosity, and pore size analyses demonstrates that MXene loading directly governs nanofiber arrangement, inter-fiber voids, and membrane microstructure, establishing the foundation for filtration performance [16,17].

Surface Chemistry and Hydrophilicity

Fourier Transform Infrared Spectroscopy (FTIR) and Energy-dispersive X-ray analysis (EDX) analysis confirmed successful incorporation of MXene into PVDF nanofibers and revealed its effect on surface chemistry (Figures 8–9, Table 1). FTIR spectra showed characteristic PVDF bands (650–900 cm^{-1}) alongside C–O (1000–1450 cm^{-1}), C=O (1700–1750 cm^{-1}), and C≡C/C=C (2100–2250 cm^{-1}) vibrations associated with MXene. PVDF-M 3% exhibited minimal residual N–H signals, indicating efficient solvent removal and clean surface chemistry.

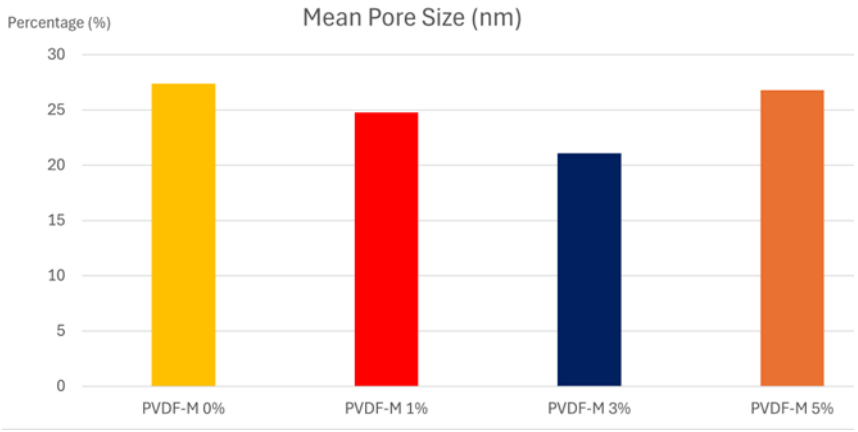

Figure 7. Data analysis for membrane mean pore size.

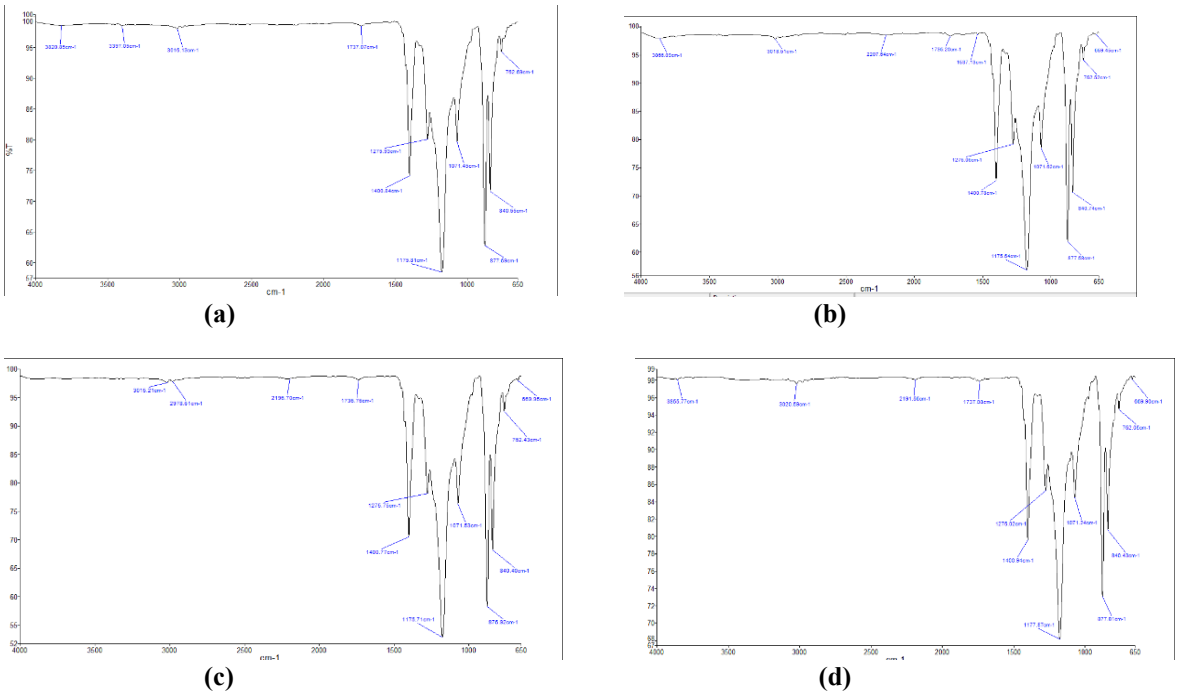

Figure 8. FTIR analysis illustrating the type of groups detected on the PVDF-MXene nanofibers membranes at different ratios: (a) PVDF-M 1%, (b) PVDF-M 3% and (c) PVDF-M 5%.

Table 1. Data analysis for FTIR wavelength range on the PVDF-MXene membranes at different loadings.

Samples (wt%)	Wavelength range (cm^{-1})	Functional Group
PVDF-M 0 wt%	762.69	Aromatic group (C-H)
	840.65	Aromatic group (C-H)
	877.69	Aromatic group (C-H)
	1071.45	Alcohol group (C-O)
	1175.81	Ether group (C-O)
	1275.93	Ether group (C-O)
	1400.84	Ether group (C-O)
	1737.07	Aldehyde group (C=O)
	3016.13	Alkene group (C-H)
	3397.05	Amine group (N-H)
	3820.85	Amine group (N-H)
PVDF-M 1.0 wt%	669.45	Aromatic group (C-H)
	762.52	Aromatic group (C-H)
	840.74	Aromatic group (C-H)
	877.58	Alcohol group (C-O)
	1071.62	Ether group (C-O)
	1175.64	Ether group (C-O)
	1276.06	Ether group (C-O)
	1400.78	Ether group (C-O)
	1537.13	Alkene group (C=C)
	1736.20	Aldehyde group (C=O)
	2207.64	Alkynes group (C≡O)
	3018.61	Methyl group (C-H)
	3866.09	Amine group (N-H)
PVDF-M 3.0 wt %	**669.95**	**Aromatic group (C-H)**
	762.43	**Aromatic group (C-H)**
	840.40	Aromatic group (C-H)
	876.92	Alcohol group (C-O)
	1071.53	Alcohol group (C-O)
	1175.71	Ether group (C-O)
	1275.75	Ether group (C-O)
	1400.77	Ether group (C-O)
	1736.76	Aldehyde group (C=O)
	2196.70	Alkyne group (C≡C)
	2978.61	Methyl group (C-H)
	3015.21	Methyl group (C-H)
PVDF-M 5.0 wt%	669.90	Aromatic group (C-H)
	762.05	Aromatic group (C-H)
	840.43	Aromatic group (C-H)
	877.81	Alcohol group (C-O)
	1071.24	Alcohol group (C-O)
	1177.87	Ether group (C-O)
	1276.02	Ether group (C-O)
	1400.94	Ether group (C-O)
	1737.08	Aldehyde group (C=O)
	2191.56	Alkyne group (C≡C)
	3020.59	Methyl group (C-H)
	3855.77	Amine group (N-H)

(a)

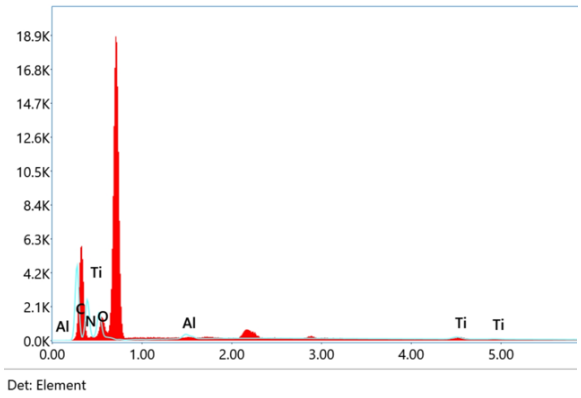

Element	Weight %	Atomic %	Error %
C K	41.06	46.28	9.58
N K	37.78	36.49	11.54
O K	19.79	16.74	12.09
Al K	0.48	0.24	8.34
Ti K	0.89	0.25	15.17

(b)

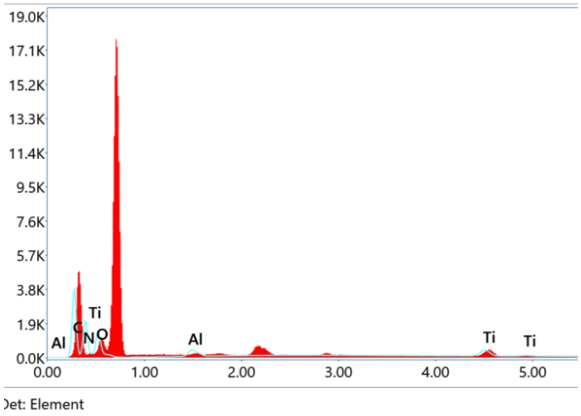

Element	Weight %	Atomic %	Error %
C K	41.00	46.88	9.77
N K	36.00	35.29	11.82
O K	19.37	16.62	12.25
Al K	0.75	0.38	7.61
Ti K	2.88	0.83	7.47

(c)

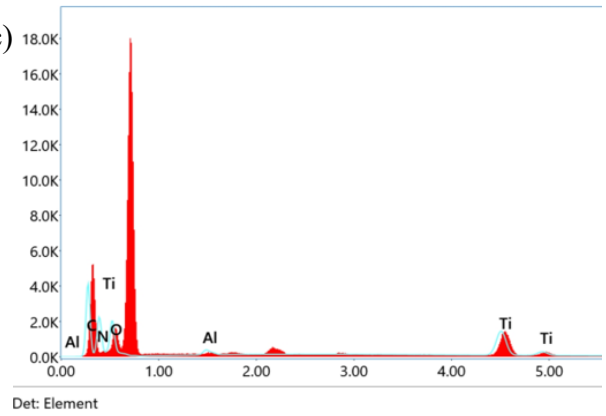

Element	Weight %	Atomic %	Error %
C K	38.04	46.04	9.83
N K	29.40	30.50	11.69
O K	22.26	20.22	11.96
Al K	0.48	0.26	9.08
Ti K	9.82	2.98	3.30

Figure 9. EDX analysis illustrating the type of groups detected on the PVDF-MXene nanofibers membranes at different ratios, (a) PVDF-M 1%, (b) PVDF-M 3% and (c) PVDF-M 5%.

EDX revealed that Ti content increased proportionally with MXene loading, confirming successful incorporation. Interestingly, PVDF-M 3% showed slightly lower bulk oxygen than PVDF-M 1% and 5%, suggesting that uniform MXene dispersion, rather than overall oxygen content, optimizes surface hydrophilicity and functional group exposure for water interaction. The clusters with agglomeration reduce the effective surface area available for water interaction and block the pore entrances. Consequently, it limits the practical contribution of oxygenated functional groups to wettability and mass transfer despite their higher abundance [18,19].

Contact angle measurements corroborated these findings, showing a decrease in water contact angle with increasing MXene loading. PVDF-M 3% achieved an optimal hydrophilicity that balances water permeability, fouling resistance, and mechanical robustness [20]. In contrast, PVDF-M 5% became excessively hydrophilic, risking polymer swelling and pore structure disruption.

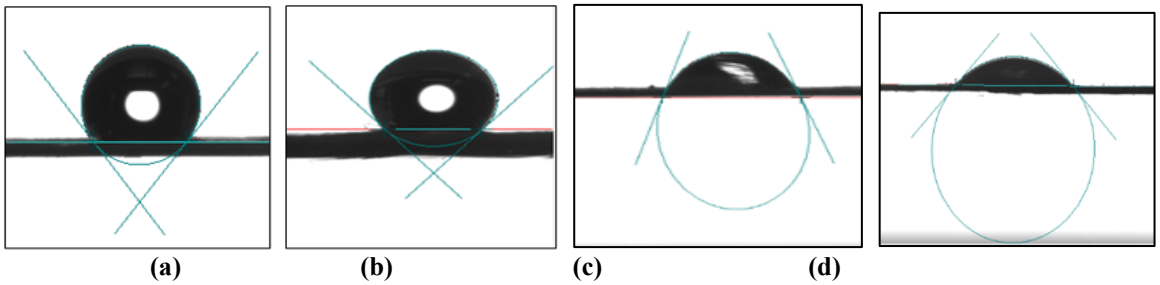

Figure 10. Contact angle readings for PVDF- MXene membranes at different loadings of MXene: a) PVDF-MXene 0 wt%, b) PVDF-MXene 1 wt%, c) PVDF-MXene 3 wt%, and d) PVDF-MXene 5 wt%.

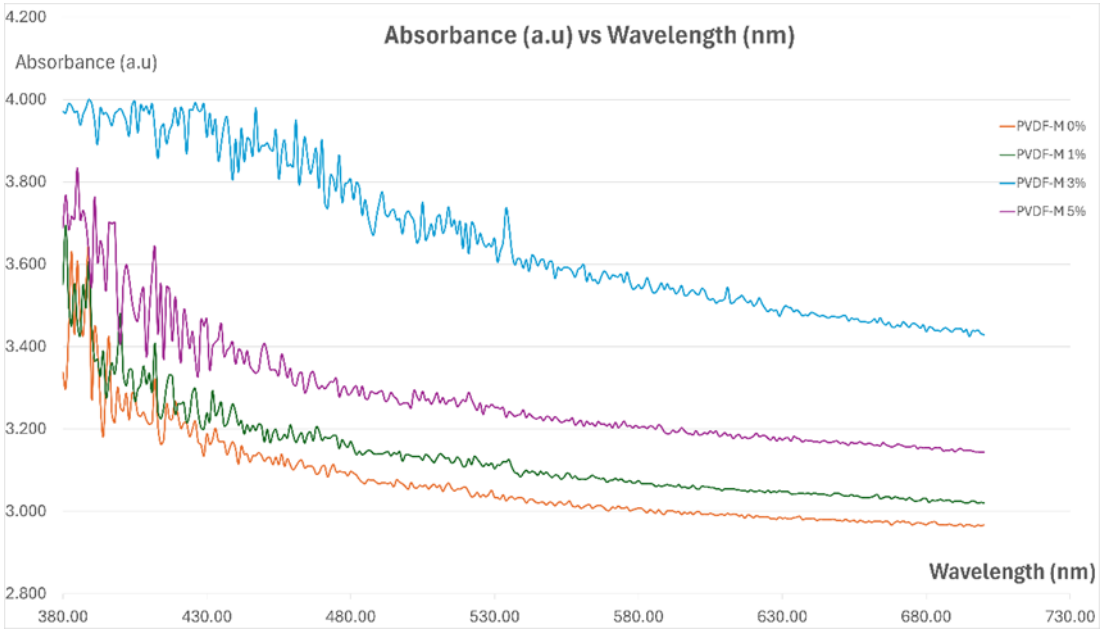

Figure 11. UV-Vis spectra analysis illustrating the absorption of PVDF-MXene nanofibers membranes at different ratios, (a) PVDF-M 1%, (b) PVDF-M 3% and (c) PVDF-M 5%.

Optical Properties and Photocatalytic Relevance

The UV-Vis spectroscopy analysis in Figure 11 demonstrated that MXene incorporation introduced broad absorption in the visible region, absent in pristine PVDF. Among all samples, PVDF-M 3% exhibited the highest absorption intensity, followed by PVDF-M 5%, and PVDF-M 1%. The strong absorption in 3% MXene loading was attributed to electronic transitions within the MXene material, particularly $n \rightarrow \pi$ transitions from functional groups like -OH or -C=O present on the MXene surface [21]. Excessive loading (PVDF-M 5%) caused light-shielding due to agglomeration, limiting photon penetration and reducing photocatalytic efficiency. Therefore, PVDF-M 3% provides the most effective exposure of photoactive sites, facilitating photocatalytic degradation of organic pollutants in POME.

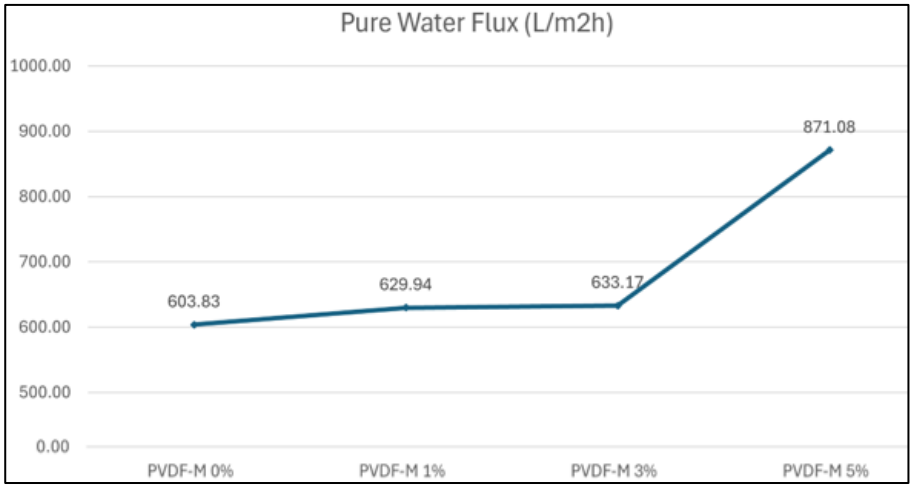

Figure 12. Water Flux Analysis.

Filtration Performance

Water flux, POME flux, chemical oxygen demand (COD) rejection, and total suspended solid (TSS) results are summarized in Figures 12 to 15. Water and POME flux increased with MXene loading due to enhanced hydrophilicity and porosity. PVDF-M 5% exhibited the highest flux but compromised filtration selectivity due to enlarged pores and nanosheet agglomeration [20]. In contrast, PVDF-M 3% provided a balanced flux while maintaining effective COD and TSS rejection.

COD rejection followed the order PVDF-M 1% > PVDF-M 3% > PVDF-M 5% > PVDF-M 0%, highlighting the combined influence of pore size and surface chemistry. PVDF-M 3% provided a high COD removal while maintaining greater permeability than PVDF-M 1%, achieving an optimal balance between contaminant retention and water flux. Consistently, TSS analysis showed that PVDF-M 3% exhibited superior particle removal, attributable to its uniform pore distribution and interconnected nanofiber network, which minimized localized fouling and ensured even flow through the membrane.

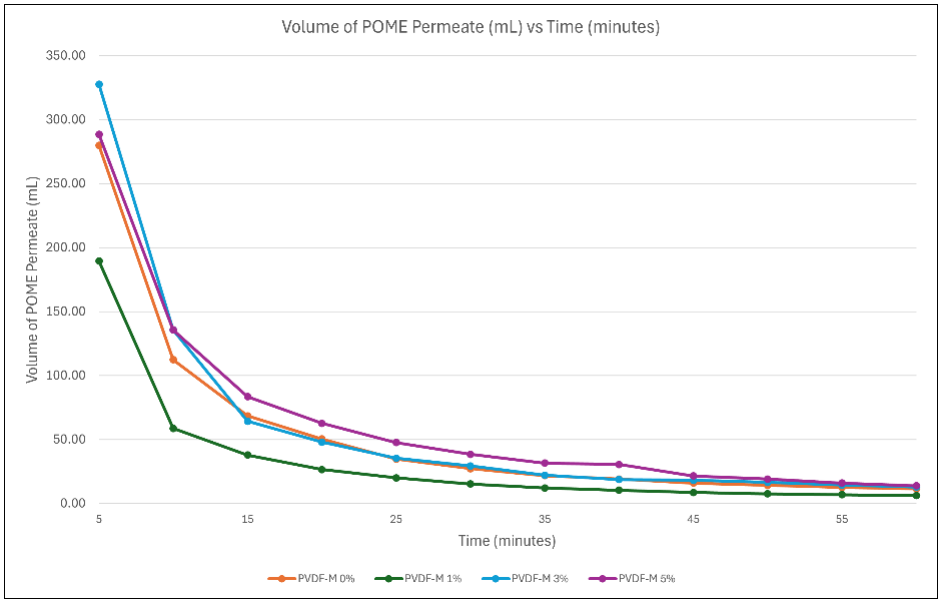

Figure 13. POME Flux Analysis.

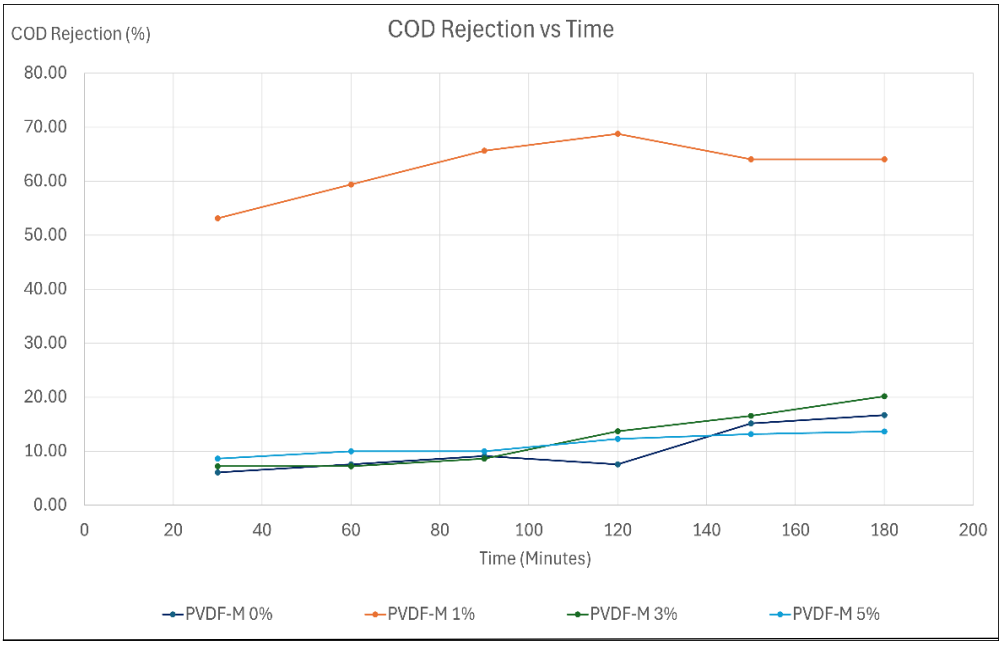

Figure 14. COD Rejection Analysis.

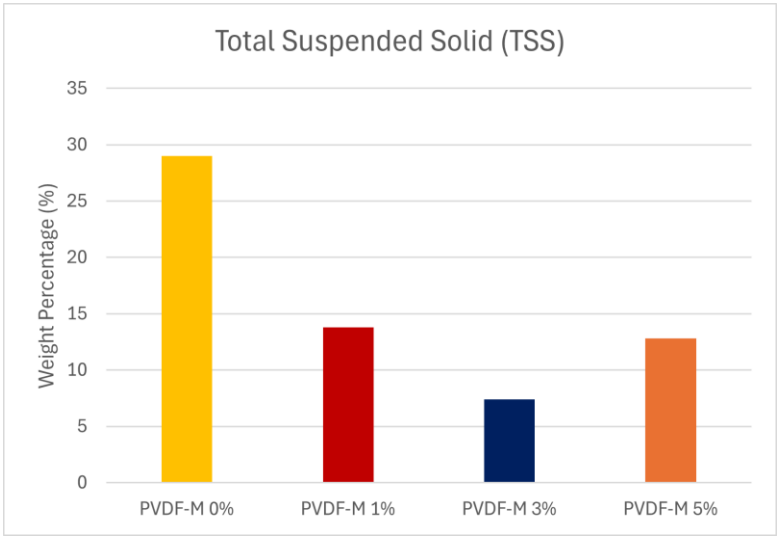

Figure 15. Total Suspended Solid Analysis.

CONCLUSION

In this work, MXene-immobilized PVDF (PVDF-M) nanofiber membranes with varying MXene loadings (0–5 wt%) were successfully fabricated and evaluated for palm oil mill effluent (POME) treatment. SEM, porosity, pore size, FTIR, EDX, and contact angle analyses revealed that MXene effectively tuned the structural and functional properties of the PVDF membrane, enhancing nanofiber diameter, surface wettability, and light absorption. This structural and chemical modification translated into improved water and POME flux as well as higher contaminant removal efficiency. Among all membranes, PVDF-M 3% demonstrated the most balanced performance, combining high COD and TSS removal with uniform pore structure, strong hydrophilicity, and minimal MXene agglomeration. While PVDF-M 1% achieved the highest COD rejection, its lower flux limited practical applicability, whereas excessive MXene loading (5%) caused pore enlargement and aggregation, reducing separation efficiency. These findings highlight the potential of MXene-immobilized PVDF membranes as a scalable and sustainable platform

for advanced POME treatment and other industrial wastewater applications.

ACKNOWLEDGEMENTS

The author acknowledge Universiti Teknologi Malaysia (UTM) for financial support and research facilities.

REFERENCES

1. Ezechi, H., Ezerie and Muda, K. (2019) Overview of trends in crude palm oil production and economic impact in Malaysia. *Sriwijaya Journal of Environment*, **4(1)**, 19–26.

2. Kristanti, R. A., Hadibarata, T., Yuniarto, A. and Muslim, A. (2021) Palm oil industries in Malaysia and possible treatment technologies for palm oil mill effluent: A review. *Environmental Research, Engineering and Management*, **77(3)**, 50–65.

3. Ahmad, A. L., Ismail, S. and Bhatia, S. (2005) Membrane treatment for palm oil mill effluent: Effect of transmembrane pressure and crossflow velocity. *Desalination*, **179**, 245–255.

4. Dong, H., Zeng, G., Tang, L., Fan, C., Zhang, C., He, X. and He, Y. (2015) An overview on limitations of TiO2-based particles for photocatalytic degradation of organic pollutants and the corresponding countermeasures. *Water Research*, **79**, 128–146.

5. Moma, J. and Baloyi, J. (2018) Photocatalysts - Applications and Attributes. *IntechOpen, London*.

6. Biswal, L., Mohanty, R., Nayak, S. and Parida, K. (2022) Review on MXene/TiO_2 nanohybrids for photocatalytic hydrogen production and pollutant degradations. *Journal of Environmental Chemical Engineering*, **10**, 107211.

7. Chaudhari, N. K., Jin, H., Kim, B., Baek, D. S., Joo, S. H. and Lee, K. (2017) MXene: An emerging two-dimensional material for future energy conversion and storage applications. *Journal of Materials Chemistry A*, **5**, 24564–24579.

8. Shahzad, F., Iqbal, A., Kim, H. and Koo, C. M. (2020) 2D transition metal carbides (MXenes): Applications as an electrically conducting material. *Advanced Materials*, **32**, 2002159.

9. Pandey, R. P., Rasheed, P. A., Gomez, T. A., Azam, R. S. and Mahmoud, K. A. (2020) A fouling-resistant mixed-matrix nanofiltration membrane based on covalently cross-linked Ti_3C_2TX (MXene)/cellulose acetate. *Journal of Membrane Science*, **607**, 118139.

10. Nor, N. A. M., Jaafar, J., Ismail, A. F., Mohamed, M. A., Rahman, M. A., Othman, M. H. D., Lau, W. J. and Yusof, N. (2016) Preparation and performance of PVDF-based nanocomposite membrane consisting of TiO_2 nanofibers for organic pollutant decomposition in wastewater under UV irradiation. *Desalination*, **391**, 89–97.

11. Liu, F., Hashim, A., Liu, Y., Moghareh Abed, M. R. and Li, K. (2011) Progress in the production and modification of PVDF membranes. *Fuel and Energy Abstracts*, **375(1)**, 1–27.

12. Liang, S., et al. (2013) Highly hydrophilic polyvinylidene fluoride (PVDF) ultrafiltration membranes via post-fabrication grafting of surface-tailored silica nanoparticles. *ACS Applied Materials & Interfaces*, **5(14)**, 6694–6703.

13. Sounderajan, S., Rajan, J. S. and Ling, J. (2022) Synthesis of MXene-PVDF composite nanofiber cloth. *Current Science and Technology*, **2(1)**, 1–11.

14. Mokhtar, N. M., Lau, W. J., Ismail, A. F. and Ng, B. C. (2014) Physicochemical study of polyvinylidene fluoride–Cloisite15A composite membranes for membrane distillation application. *RSC Advances*, **4**, 63367–63379.

15. Al-Dhahebi, A., Rebecca, L., Nuge, T. and Shuaib, M. (2023) Effects of Ti_3C_2Tx MXene nanofillers on the rheological and morphological characteristics of electrospun PVDF nanofibers. In *2023 IEEE International Conference on Sensors and Nanotechnology (SENNANO), Putrajaya*, 228-232.

16. Abood, T. W., Shabeeb, K. M., Alzubaydi, A. B., Fal, M., Lotaibi, A. M., Lawal, D. U., Hernadi, K. and Alsalhy, Q. F. (2024) Novel MXene/PVDF nanocomposite ultrafiltration membranes for optimized Eriochrome black T (azo dye) removal. *Desalination and Water Treatment*, **318**, 100311.

17. Feng, L., Zhang, Z., Mai, Z., Ma, Y., Liu, B., Jiang, L. and Zhu, D. (2004) A super-hydrophobic and super-oleophilic coating mesh film for the separation of oil and water. *Angewandte Chemie International Edition*, **43(15)**, 2012–2014.

18. Wang, H. (2023) Enhanced degradation of tetracycline via visible-light-assisted peroxymonosulfate activation over oxygen vacancy-rich Fe_2O_3-$CoFe_2O_4$ heterostructures.

Separation and Purification Technology, **314**, 123586.

19. Mafirad, S., Mehrnia, M. R., Azami, H. and Sarrafzadeh, M. H. (2011) Effects of biofilm formation on membrane performance in submerged membrane bioreactors. *Biofouling*, **27(5)**, 477–485.

20. Abood, T. W., Shabeeb, K., Alzubaydi, A. B., Goh, P. S., Ismail, A. F., Zrelli, A. and Alsalhy, Q. F. (2024) Effect of MXene Ti_3C_2 on the PVDF ultrafiltration membrane properties and performance. *Engineering and Technology Journal*, **42(6)**, 754–767.

21. Adomavičiūtė-Grabusovė, S., Ramanavičius, S., Popov, A., Šablinskas, V., Gogotsi, O. and Ramanavičius, A. (2021) Selective enhancement of SERS spectral bands of salicylic acid adsorbate on 2D Ti_3C_2Tx-based MXene film. *Chemosensors*, **9(8)**, 223.